Influence of boundaries on magnetic ordering in Fe/V superlattices

Martina Ahlberg, Moreno Marcellini, Andrea Taroni, Gabriella Andersson, Maximilian Wolff, and Björgvin Hjörvarsson
Department of Physics and Astronomy, Uppsala University, P.O. Box 516, SE-751 20 Uppsala, Sweden
(Received 10 March 2010; revised manuscript received 1 June 2010; published 18 June 2010)

We study the role of surface boundaries on the magnetic properties of $[Fe/V]_n$ superlattice structures, with $n=2-10$. Using the magneto-optical Kerr effect and polarized neutron reflectivity measurements, we examine the evolution of both the total and the layer-resolved magnetizations as a function of temperature. By varying n, we observe a large shift in the transition temperatures T_c and a substantial change in the total magnetization critical exponent β. In particular, the thicker samples exhibit nonuniversal exponent values. By resolving the magnetization as a function of position within the superlattice, we show that this behavior arises from contributions of the surfaces. Furthermore, we attribute the large shift in T_c to long-ranged interactions present in the superlattice.

DOI: 10.1103/PhysRevB.81.214429 PACS number(s): 75.70.Cn, 75.70.Rf, 75.40.Cx

I. INTRODUCTION

Surface and interface boundaries play an important role in magnetic nanoscale structures.[1–3] Near a surface, the magnetization is suppressed relative to the bulk, and ordering takes place in response to the establishment of the bulk magnetization. If the layer is sufficiently thin, this leads to a noticeable reduction in the magnetization and a concomitant reduction in the ordering temperature.[4,5] It is therefore common to observe a substantial suppression in the ordering temperature, relative to the bulk value, for systems thinner than a few tens of nanometers.[6–9]

Close to the transition temperature T_c of a continuous phase transition the magnetization may be described in terms of a power law, $M \propto (1-T/T_c)^{\beta}$, where β is a critical exponent.[10] The value of β is indicative of the universality class to which the system belongs, which in turn is dictated by the spatial dimensionality of the system and the symmetry of the order parameter, as well as the range of the interactions present. In the context of magnetism, this implies a classification according to the lattice and spin dimensionality of the system.

The theory of critical phenomena can be extended in order to include the presence of surface boundaries.[4,11,12] The revised theory successfully predicts surface exponents that are drastically different from their bulk counterparts. For example, the so-called *ordinary transition* for the Heisenberg model, which arises provided couplings are not for some reason altered at the surface, is predicted to have surface and bulk magnetization exponents corresponding to $\beta_s=0.84$ and $\beta_b \simeq 0.32$.[13] This is consistent with Monte Carlo simulations[4,5] and experimental work by Arnold and Pappas,[14] who determined the critical exponents of the surface and bulk in Gd to be $\beta_s=0.83\pm0.04$ and $\beta_b=0.376\pm0.015$, respectively.

When a magnetic film is thin enough, it effectively consists of two merged surface regions. The characteristic signature of this is a magnetization that, for temperatures approaching T_c, varies as a function of layer index. Compelling experimental evidence of such an effect has, for example, been measured using Mössbauer spectroscopy in Fe/W(110) thin films[15] and, more recently, in EuTe(111) films using resonant soft x-ray diffraction.[16] However, the influence surfaces have on the overall behavior of thin magnetic structures, and superlattices in particular, is not well understood. For instance, the observation of large shifts in the transition temperature with increasing thickness of the films,[6,8,17] along with that of abnormally high bulk exponent values,[18] is in contradiction with the established theoretical predictions for low-dimensional systems.

In this work, we investigate the influence of surface boundaries on the magnetic behavior of $[Fe/V]_n$ superlattices. We focus on effects arising from the number of magnetic Fe layers and the position of the layers within the superlattices, where we adopt the term *layer* to denote a sheet of Fe consisting of three atomic monolayers (ML). We use the magneto-optical Kerr effect (MOKE) to study the magnetization as a function of temperature, which allows us to obtain the critical temperature T_c and exponent β for different numbers of repetitions, n. Polarized neutron reflectivity (PNR) is used to measure the evolution of the magnetization as a function of position, i.e., the spatially resolved magnetic profile, and of temperature. We argue that in order to account for our observations in a consistent manner, a nearest-neighbor theory must be abandoned in favor of one in which long-range interactions are explicitly included.

II. EXPERIMENTAL

A. Sample growth

Three different sets of Fe/V superlattices, which we refer to as sets A, B, and C, were grown according to the recipe outlined by Isberg *et al.*[19] Set A consists of a series of superlattices with the structure $[Fe(3)/V(9)]_n$, where n is the number of repetitions and the number within brackets denotes the number of monolayers, whereas the superlattices in set B have the structure $[Fe(3)/V(10)]_n$. The samples were grown in a random order to detect any influence of drifting growth rate on the critical temperature of the superlattices. A schematic illustration of these superlattice structures is displayed in Fig. 1.

We have also manufactured a somewhat more complicated system, with the structure *substrate*/V(9)/$[SL_1/SL_2]_{15}$.

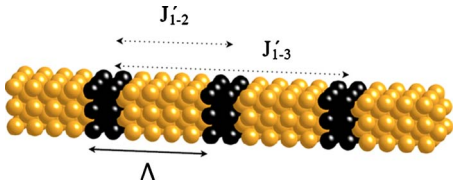

FIG. 1. (Color online) Schematic illustration of a $[Fe(3)/V(9)]_n$ superlattice with $n=3$, in which the repetition distance Λ and the interlayer coupling $J'_{i,k}$ are defined.

Here, SL_1 denotes the sequence $[Fe(3)/V(9)]_4/Fe(3)$, and SL_2 denotes V(12)/Fe(1)/V(10)/Fe(1)/V(12). System C therefore consists of a repeated sequence of two superlattices, and we term this structure a *super*-superlattice. The iron in SL_2 is present solely for the benefit of the growth process and minimizes the thickness variation between the magnetic superlattices. SL_2 provides a magnetic *decoupling* between the SL_1 superlattices since 1 ML of iron embedded in vanadium is not ferromagnetic at any temperature.[20] All the samples we prepared were grown on MgO(001) substrates and covered by a Pd capping layer ($\approx$35 Å) to avoid oxidation. X-ray reflectivity was used to determine the sample quality.

As part of our study, we performed MOKE measurements in order to investigate the change in the transition temperature $T_c(n)$ and the critical exponent β, as a function of n, for the samples in sets A and B. System C was prepared in order to allow us to examine the spatially resolved magnetic profile of a magnetic system as a function of temperature, which we achieved through PNR measurements.

B. MOKE measurements

The magnetization of all the samples was investigated as a function of temperature using a MOKE setup, described in Ref. 20. The samples were mounted on an optical cryostat which, depending on temperature range of interest, is cooled with liquid nitrogen or helium. The cryostat is shielded by three layers of μ metal to reduce stray fields. A 5 Hz alternating magnetic field generated by a pair of Helmholtz coils was applied, and hysteresis loops were continuously recorded while varying the temperature with a cooling rate of 0.2 K/min to ensure thermal equilibrium. Measurements recorded during 30 s were averaged to give one final hysteresis loop. From this series of hysteresis loops, we extracted the remanent magnetization as a function of temperature.

C. Neutron reflectivity

The super-superlattice (system C) was studied using polarized neutron reflectivity performed at the ADAM reflectometer at the Institute Laue-Langevin in Grenoble, France.[21] Supermirrors and Mezei-type coils, which flip the neutron spin by π rad, were used in the incident beam for polarization. The polarization efficiency was determined to be above 0.95. The measurements were carried out in an angle dispersive mode at a wavelength of 4.41 Å and a resolution $\Delta\lambda/\lambda=0.006$. The incident beam collimation was fixed at 0.03°. The sample was measured inside a He cryostat, and for obtaining a magnetic field perpendicular to the scattering plane, an electromagnet ($-0.7 \leq H_y \leq 0.7$ T) with a laminated iron yoke was used. The moment of the neutron is then parallel to the external field, which is defined as the y direction.

In a scattering experiment, the scattering potential is given by a periodic function, which may be described as a Fourier series,

$$f(x) = \frac{u_0}{2} + \sum_{i=1}^{\infty} [u_i \cos(ix) + v_i \sin(ix)], \tag{1}$$

where the coefficients are given by

$$u_i = \frac{1}{\pi}\int_0^{2\pi} f(x)\cos(ix)dx, \quad i = 0,1,2,\ldots, \tag{2}$$

$$v_i = \frac{1}{\pi}\int_0^{2\pi} f(x)\sin(ix)dx, \quad i = 1,2,\ldots. \tag{3}$$

This expression holds in the absence of multiple scattering, which is reasonable in the case of neutron experiments on thin films, in which even single scattering events are rare.

Typically, one measures the Fourier transform of the scattering potential, with each Bragg peak corresponding to one component of the Fourier series. It is, however, impossible to distinguish between the cosine and sine components since only their amplitudes are measured and the phase information is lost. One way around this problem is to manufacture a sample that can be described *only* by a cosine series, i.e., a periodic step function

$$f(x) = \begin{cases} 1, & \pi/3 \leq x \leq 5\pi/3 \\ 0, & \text{elsewhere}. \end{cases} \tag{4}$$

In a PNR experiment, the scattering potential is related to both the magnetic and chemical variations of the sample. The magnetic contribution to the scattering is reflected by the spin asymmetry,

$$S = \frac{I^{\uparrow} - I^{\downarrow}}{I^{\uparrow} + I^{\downarrow}}, \tag{5}$$

where I is the integrated intensity of the spin-up and spin-down reflectivities. To a first approximation, S is proportional to the product of projection of the magnetization along the y axis, M_y, and the contrast in nuclear scattering length, b: $S \propto \Delta b M_y$, where $\Delta b = b_{Fe} - b_V$.[22–24] It therefore reflects the magnetic contribution to the scattering. The spin asymmetry of each Bragg peak, S_i, reproduces the magnitude of the corresponding Fourier component of the magnetic profile.

III. RESULTS

A. Critical temperature—n dependence

The energy scale which determines the critical temperature of a single ferromagnetic layer is dictated by the intralayer coupling constant J.[10] Superlattices are characterized by two additional degrees of freedom, which are the number

of layer repetitions, n, and the interlayer exchange coupling (IEC) between different layers, J'. The IEC occurs through an indirect exchange mechanism that is closely related to the Ruderman-Kittel-Kasuya-Yosida (RKKY) interaction and is therefore oscillatory in nature.[1] In the case of Fe/V superlattices, the IEC between the Fe layers has been mapped out with a high degree of consistency[25–28] and is known to change sign at around 11 ML of spacer distance.[18,29] For the case of our sets A and B, which correspond to spacer distances of 10 and 9 ML, respectively, the ratio J'/J is therefore rather small, on the order of 10^{-3}.[18]

In bulk magnetic systems, a small J'/J ratio is known to restrict two-dimensional fluctuations to an effective length scale corresponding to $L_{\mathrm{eff}} \sim \sqrt{J/J'}$.[31,32] This ensures two-dimensional thermodynamic behavior, even in a system for which $n \to \infty$, up until very close to T_c, whereupon a crossover to three-dimensional behavior occurs. In the two-dimensional limit, a thin film of 3 ML Fe, embedded in V, is known to belong to the two-dimensional XY (2dXY) universality class.[30] The critical temperature of a 2dXY system of effective size L_{eff} is given by[31]

$$T_c(L_{\mathrm{eff}}) \approx T_{\mathrm{KT}} + \frac{\pi^2}{c[\ln(L_{\mathrm{eff}})]^2}, \tag{6}$$

where T_{KT} is the Kosterlitz-Thouless temperature ($\approx 0.898 J/k_B$) [33] and c is a constant [≈ 2.1 (Ref. 34)].

In a superlattice, the outermost layers are characterized by having only one neighboring layer, whereas the central layers have two. This implies an effective interlayer coupling that is half as big at the surface, compared to the interior of the sample. Using Eq. (6) we can calculate the difference in critical temperature between the two limiting cases of $n=2$ and $n=\infty$, where $J'_{n=\infty} = 2J'_{n=2}$. The ratio J/J' dictates the possible shift in T_c. A value of $L_{\mathrm{eff}} = J/J' = 10^3$ gives an increase of 8%, while a relatively small value of $J/J' = 70$ still results in a modest increase of 23%.

Figure 2 displays the critical temperatures as a function of n, measured for the samples in sets A and B using the MOKE technique. The $[\mathrm{Fe}(3)/\mathrm{V}(9)]_n$ samples display lower T_c values than the $[\mathrm{Fe}(3)/\mathrm{V}(10)]_n$ samples, a fact that is seemingly in contradiction with the nominal values of their Fe layer thicknesses (d_{Fe}). However, we note that the growth rate is recalibrated before each series is manufactured; consequently, we expect d_{Fe} to differ slightly between different series since even the slightest changes in d_{Fe} are known to have a large impact on T_c in thin superlattices.[17] Nevertheless, the fast shutter speed in the preparation chamber ensures a constant d_{Fe} within the same series.

The shift we observe in $T_c(n)$ of series A is of nearly 200 K, corresponding to an increase of roughly 400%. Using $n=2$ as reference, the shift is about 125%. Clearly, this shift is grossly underestimated by Eq. (6). We argue that this discrepancy can be bridged by considering long-range interactions. This can be demonstrated within a mean-field approximation, in which we assume that the critical temperature is proportional to the average IEC within the superlattice, $T_c \propto \langle J' \rangle$, and that the coupling between two layers i and k decays algebraically with distance as $J'_{ik} \propto |r_i - r_k|^{-\alpha}$, where α

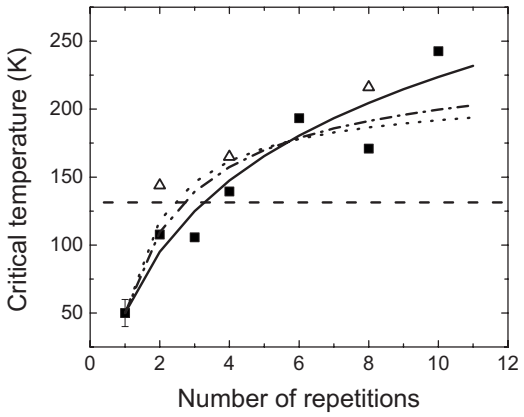

FIG. 2. The critical temperature of $[\mathrm{Fe}(3)/\mathrm{V}(9)]_n$ (filled squares) and $[\mathrm{Fe}(3)/\mathrm{V}(10)]_n$ (open triangles) superlattices versus the number of repetitions, n. The dashed horizontal line indicates the highest critical temperature obtained using Eq. (6) with $J/J' = 70$, which is based on nearest-neighbor considerations. The continuous, dashed-dotted, and dotted lines correspond to values of $\alpha = 1$, 2, and 3 in expression (7), which heuristically assumes long-range interactions. See main text for details.

is a parameter reflecting the range of the interaction. The average coupling within the sample is therefore the sum of all the couplings between layers, normalized to n, $\langle J' \rangle = \frac{1}{n} \Sigma J'_{ik}$. Assuming that a single magnetic layer has an ordering temperature $T_c(n=1)$, the shift in T_c with n is

$$T_c(n) = T_c(n=1) + \frac{a}{2n} \sum_{i,k}^{n} \frac{1}{|r_i - r_k|^{\alpha}}, \tag{7}$$

where a is some constant and the factor of 1/2 excludes double counting. This expression captures the overall changes in $T_c(n)$, and it has the merit of providing a qualitative explanation for the large increase in the ordering temperature as a function of n, as illustrated in Fig. 2. Equation (7) is similar to derivations of the strength of interlayer coupling in multilayers, which decays as d_s^{-2} for transition metals, where d_s is the spacer thickness.[35] In the calculations only trilayer structures were considered and one can expect deviations from the relation above when summing over several magnetic layers. We can therefore not draw any conclusions from the value of α.

Furthermore, we observe oscillations in T_c when the sample thickness increases. This observation was reproduced by measurements on an additional set of samples similar to series A. J' is known to be an oscillatory function of spacer thickness (d_s),[36] cap layer thickness (d_{cl}),[37] and magnetic layer thickness.[38] Concomitant alternations in critical temperature are found primarily when d_s is varied,[39] but also as a function of d_{cl}.[40] Further investigation of these oscillations, which we believe are related to quantum confinement effects that result in a modification of the density of states,[41] is deferred for future work.

B. Critical behavior—n dependence

We estimated the critical exponent β for each sample in sets A and B, by analyzing the magnetization data we ob-

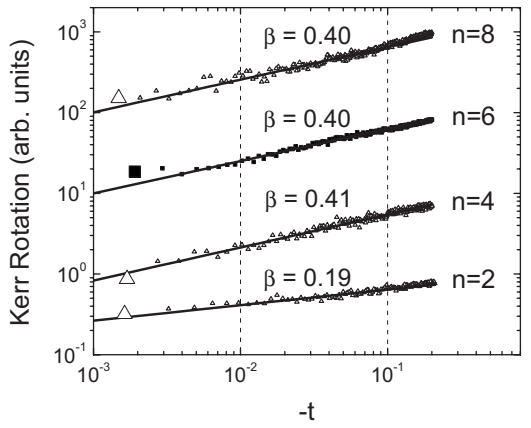

FIG. 3. Magnetization data of $[\mathrm{Fe}(3)/\mathrm{V}(10)]_n$ (open triangles) and $[\mathrm{Fe}(3)/\mathrm{V}(9)]_6$ (filled squares) superlattices plotted in a log-log scale. The first data markers are enlarged for clarity. The solid lines correspond to linear fits performed within the interval $0.01 \leq -t \leq 0.1$, indicated by the dashed vertical lines.

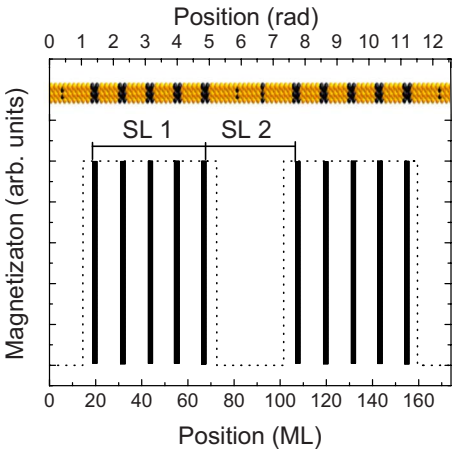

FIG. 4. (Color online) A schematic illustration of the magnetic periodicity of the super-superlattice sample. The dotted line represents the overall magnetic profile and the bars show the magnetization in the Fe layers of SL_1.

tained from MOKE using the method described by Elmers *et al.*[42] This involves fitting the experimental data to the power law $M \propto (1-T/T_c)^{\beta}$ and convoluting it with a Gaussian distribution of critical temperatures, in order to capture the rounded tail of the magnetization curve. To verify our fits, we also used the obtained T_c values to plot $\log_{10}(M)$ versus $\log_{10}(-t)=\log_{10}(1-T/T_c)$, as shown in Fig. 3.

For the $n=2$ sample, we measure an exponent of $0.19 \leq \beta \leq 0.26$ consistent with the 2dXY model, and in agreement with previous reports in the literature.[30] For larger values of n, we find a concomitant increase to values of $0.32 \leq \beta \leq 0.41$ resembling a range expected for a three-dimensional Heisenberg system. Although it is tempting to associate this with a crossover from two- to three-dimensional critical behavior, the low value of the ratio J'/J excludes this possibility. Instead, we trace the change in the effective exponent to the nonhomogenous changes in the layer specific magnetization. This is described in the next section.

C. Layer specific magnetization

The layer specific magnetization was obtained by using a specially designed sample, illustrated in Fig. 4. At low temperature, we initially assume that all the Fe layers in the super-superlattice sample have the same magnetization. In order to determine the temperature dependence of this initially squarelike magnetization profile, we monitor the spin asymmetry of the Bragg peaks arising from the super-superlattice structure. In practice, the number of accessible Fourier components is limited since the Fourier sum can only include the number of Bragg peaks in the reflectivity curve, which in our experiment is restricted to six. This corresponds to eight Fourier components since u_3 and u_6 of $f(x)$ are both equal to zero, as is readily apparent by examining Eq. (2). The evolution of the magnetic profile versus temperature is therefore given by

$$F(x,T) = \frac{u_0(T)}{2} + \sum_{i=1}^{8} u_i \cos(ix) S_i^{\mathrm{norm}}(T), \tag{8}$$

where x is the position and u_i are the Fourier coefficients of the initial scattering potential defined in Eq. (4). S_i is the spin asymmetry of the Bragg peak Q_i and S_i^{norm} is the spin asymmetry normalized to the temperature where the magnetization profile is assumed to be squarelike. Although $u_0(T)$ is not measurable, this does not pose a problem since it is not related to the shape of the profile and only represents an offset. The magnetization is zero outside the magnetic superlattice, so we can adjust the offset to ensure that $F(x,T)$ is also zero in this region, therefore avoiding any artifacts arising from u_0.

1. Simulations

In order to verify the validity of our approach, we have simulated reflectivity spectra, using the Parratt formalism,[43] of the super-superlattice for different magnetic scattering length densities in the Fe(3) layers, corresponding to different magnetizations varying with temperature. In turn, we used these spectra to reconstruct the magnetic profiles. The result of this calculation clearly demonstrates that, despite the limited number of available Fourier components, it is possible to resolve the magnetization profile using the method we have outlined.

Furthermore, Q_7 corresponds to the repetition distance Λ of SL_1 and thus the spin asymmetry of this peak is closely related to the average magnetization of the superlattice. This was confirmed by the simulations, where the spin asymmetry of Q_7 was found to scale with the average magnetization.

In real samples, it is known that the vanadium in proximity to the iron layers experiences an induced polarization that is oriented antiparallel to that of the iron.[44,45] Furthermore, this effect is enhanced in the case of rough interfaces.[46] We have therefore performed a second simulation, in which we take this effect into account by adding two magnetic vanadium layers, each 3 ML thick, around each iron layer. Since

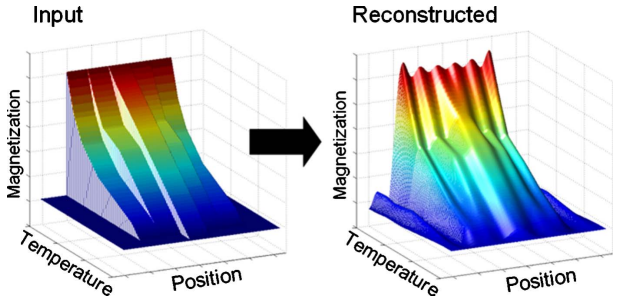

FIG. 5. (Color online) Left: magnetization profile of the Fe layers in the model sample. Right: profile reconstructed from calculated spectra which includes V polarization.

the magnetization of the vanadium layer, M_V, is caused by the interaction between Fe and V atoms, we assume that its magnitude is proportional to the magnetization of the iron, M_{Fe}. In addition, in order to capture imperfections in the Fe/V interfaces, we used the highest reported values for the induced polarization, $M_V \approx 0.3 M_{Fe}$.[46] Our model does not, however, take into account the fact that there is a larger M_V at the Fe/V interface, as opposed to the V/Fe interface.[46] The results of this second simulation are shown on the right-hand side of Fig. 5. Although the correspondence between the spin asymmetry of Q_7 and the average magnetization is less clear compared to the previous simulation, we find that the overall shape of the profile remains preserved.

2. PNR data

A representative polarized neutron reflectivity scan is displayed in Fig. 6, in which the black solid line and the red dashed line are the spin-up and spin-down measurements, respectively. The evolution with temperature of the spin asymmetry at each one of the peaks was determined from a series of similar scans. The result of this analysis is shown in Fig. 7. The first, second, and seventh Fourier components display widely differing behaviors as a function of temperature, a clear indication that the magnetization behaves differently within the individual layers of the superlattice.

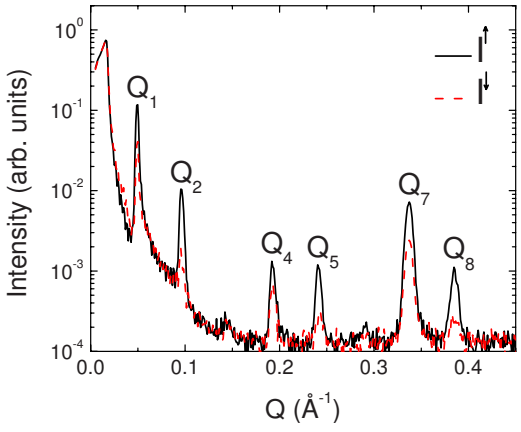

FIG. 6. (Color online) Polarized neutron reflectivity of the super-superlattice sample at 12 K. The black solid line and the red dashed line indicate the spin-up and spin-down reflectivities, respectively. The peaks are denoted by Q_i, after the corresponding Fourier component.

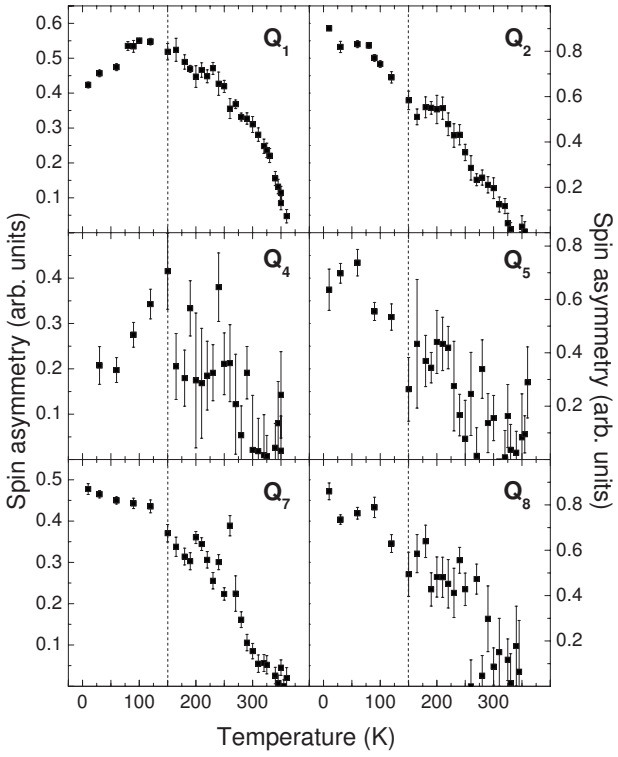

FIG. 7. The temperature dependence of the spin asymmetries of the six observed Bragg peaks. The data points, at and above 150 K, were used to calculate the magnetic profile.

The temperature evolution of the first Bragg peak Q_1, shown in Fig. 7, corresponds to the first Fourier component and is closely related to the magnetization at the center of the profile. Below 150 K, the spin asymmetry decreases, implying a suppression of the magnetization component M_y in the central layers associated with a rotation of the magnetization. This phenomenon, while interesting in itself, complicates our analysis since it invalidates the assumption of a squarelike magnetization profile at low temperature. Therefore, we only reconstruct the data above 150 K and defer to the low-temperature data analysis to future work.

The reconstructed magnetization profiles are illustrated in Fig. 8. This clearly displays a developing spatial gradient of the magnetization as the temperature increases. These observations are in agreement with the presence of magnetic surfaces with missing neighbors since the coupling in their vicinity is reduced, leading to a concomitant reduction in the magnetization. The apparent polarization of the Fe(1) layers is an artifact due to wiggles caused by the limited amount of Fourier components. This effect can also be seen in Fig. 5.

IV. DISCUSSION

The experimental facts arising from our measurements on Fe/V superlattices are the following: (i) the transition temperature increases from 50 to 245 K (approximately 400%) as n is increased from 1 to 10; (ii) within the same range of n, the critical exponent β changes from two-dimensional value of $0.19 \leq \beta \leq 0.26$ to $0.32 \leq \beta \leq 0.41$; and (iii) the

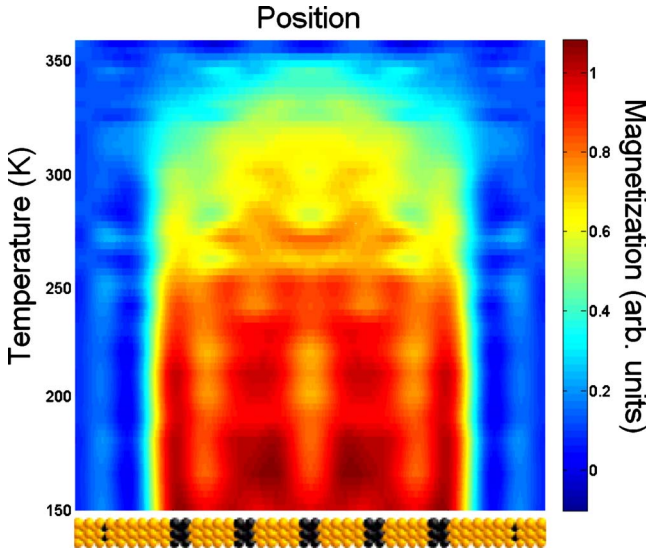

FIG. 8. (Color online) Magnetic profile of a $[Fe(3)/V(9)]_5$ superlattice calculated from PNR measurements of the super-superlattice. The corresponding atomic structure is illustrated along the x axis. The apparent magnetization in the Fe(1) layers is an artifact caused by the limited amount of Fourier components.

magnetization of the outermost layers decreases faster, as compared to the middle layer, over a wide temperature range.

Our experimental observations are in disagreement with established theory of nearest-neighbor spin models. The arguments in Sec. III lead to the conclusion that, in a system in which J'/J is small, the shift in the transition temperature should not exceed a modest increase of 8%. Furthermore, they do not predict any kind of dimensional crossover in β with increasing n since the low J'/J ratio ought to ensure two-dimensional thermodynamic behavior in the limit $n \rightarrow \infty$.[31,32] Finally, if the Fe/V superlattice system is only defined by the thickness n and the ratio J'/J, one would not expect to observe the significant surface effects in the magnetic profiles displayed in Fig. 8.

We propose a simple model including long-range interactions, which accounts for these observations in a natural manner. Long-range forces imply an enhancement of surface effects since a greater number of layers below the surface will experience a reduced coupling, compared to short-range forces. Thus, although the phenomenology of the phase transition in the vicinity of the surface, characterized by a magnetization in the outer layers decaying faster than in the middle layers of the sample, remains unchanged, its enhancement has important implications for the observed β_{eff} values of the entire sample. This follows from the fact that β_{eff} is effectively determined by an averaged sum of the β_k values associated with each individual layer k, $\beta_{\text{eff}}=\frac{1}{n}\Sigma_k^n \beta_k$.

Thus, an Fe/V superlattice may be viewed as an ensemble of layers, consisting of two merged surface regions. Each layer displays different effective exponents, as the PNR data in Fig. 8 make clear. This also gives rise to the increase in β_{eff} values that we observe for superlattices with $n>2$ and provides a plausible explanation for the abnormally high exponent values reported by Marcellini *et al.*[18] Finally, a model including long-range interactions also accounts for the large change we observe in T_c (Fig. 2).

V. CONCLUSIONS

We have investigated the magnetic behavior of $[Fe/V]_n$ superlattices using a combination of MOKE and PNR techniques. We have addressed the seemingly contradictory presence of weak interlayer exchange coupling in a system that displays a drastic change in the measured critical exponent β_{eff} and transition temperature T_c with increasing number of magnetic layer repetitions, n. Our PNR measurements on a specially fabricated super-superlattice reveal significant surface effects, which are manifested by a magnetization profile that changes as a function of layer index. We argue that the simplest model which is consistent with these experimental facts must account for the presence of long-range interactions. The plausibility of our argument is strengthened in light of the known importance of long-ranged mechanisms such as dipolar and RKKY interactions in superlattices.[1,26] It is desirable to put our qualitative findings on a more quantitative footing, perhaps by considering more realistic models in which the oscillatory and anisotropic nature of long-range interactions is taken explicitly into account.

ACKNOWLEDGMENTS

Financial support from the Swedish Science Council (Vetenskapsrådet), the Knut and Alice Wallenberg Foundation, and the German Federal Ministry for Education and Research (BMBF, Contract No. 03ZA7BOC) is gratefully acknowledged.

[1] *Ultrathin Magnetic Structures*, edited by J. A. C. Bland and B. Heinrich (Springer-Verlag, Berlin, 2005).
[2] C. A. F. Vaz, J. A. C. Bland, and G. Lauhoff, Rep. Prog. Phys. **71**, 056501 (2008).
[3] H.-J. Elmers, Int. J. Mod. Phys. B **9**, 3115 (1995).
[4] K. Binder, *Phase Transitions and Critical Phenomena* (Academic Press, London, 1983), Vol. 8, Chap. 1.
[5] K. Binder and P. C. Hohenberg, Phys. Rev. B **9**, 2194 (1974).
[6] Y. Li and K. Baberschke, Phys. Rev. Lett. **68**, 1208 (1992).
[7] F. Huang, G. J. Mankey, M. T. Kief, and R. F. Willis, J. Appl. Phys. **73**, 6760 (1993).
[8] F. Huang, M. T. Kief, G. J. Mankey, and R. F. Willis, Phys. Rev. B **49**, 3962 (1994).
[9] H. Lutz, J. D. Gunton, H. K. Schurmann, J. E. Crow, and T. Mihalisin, Solid State Commun. **14**, 1075 (1974).
[10] N. Goldenfeld, *Lectures on Phase Transitions and the Renormalization Group* (Westview Press, Colorado, 1992).
[11] M. N. Barber, *Phase Transitions and Critical Phenomena* (Academic Press, London, 1983), Vol. 8, Chap. 2.
[12] K. Binder, Ferroelectrics **73**, 43 (1987).
[13] H. W. Diehl and A. Nüsser, Phys. Rev. Lett. **56**, 2834 (1986).
[14] C. S. Arnold and D. P. Pappas, Phys. Rev. Lett. **85**, 5202 (2000).

[15] J. Korecki, M. Przybylski, and U. Gradmann, J. Magn. Magn. Mater. **89**, 325 (1990).
[16] E. Schierle, E. Weschke, A. Gottberg, W. Söllinger, W. Heiss, G. Springholz, and G. Kaindl, Phys. Rev. Lett. **101**, 267202 (2008).
[17] S. D. Bader and C. Liu, J. Vac. Sci. Technol. A **9**, 1924 (1991).
[18] M. Marcellini, M. Pärnaste, B. Hjörvarsson, G. Nowak, and H. Zabel, J. Magn. Magn. Mater. **321**, 1214 (2009).
[19] P. Isberg, B. Hjörvarsson, R. Wäppling, E. B. Svedberg, and L. Hultman, Vacuum **48**, 483 (1997).
[20] M. Pärnaste, M. van Kampen, R. Brucas, and B. Hjörvarsson, Phys. Rev. B **71**, 104426 (2005).
[21] M. Wolff, K. Zhernenkov, and H. Zabel, Thin Solid Films **515**, 5712 (2007).
[22] C. F. Majkrzak, Physica B **221**, 342 (1996).
[23] H. Zabel, Physica B **198**, 156 (1994).
[24] G. Felcher, Physica B **192**, 137 (1993).
[25] M. Vohl, J. A. Wolf, P. Grünberg, K. Spörl, D. Weller, and B. Zeper, J. Magn. Magn. Mater. **93**, 403 (1991).
[26] G. R. Harp, M. M. Schwickert, M. A. Tomaz, T. Lin, D. Lederman, E. Mayo, and W. L. O'Brien, IEEE Trans. Magn. **34**, 864 (1998).
[27] M. M. Schwickert, R. Coehoorn, M. A. Tomaz, E. Mayo, D. Lederman, W. L. O'Brien, T. Lin, and G. R. Harp, Phys. Rev. B **57**, 13681 (1998).
[28] A. Broddefalk, R. Mathieu, P. Nordblad, P. Blomqvist, R. Wäppling, J. Lu, and E. Olsson, Phys. Rev. B **65**, 214430 (2002).
[29] B. Hjörvarsson, J. A. Dura, P. Isberg, T. Watanabe, T. J. Udovic, G. Andersson, and C. F. Majkrzak, Phys. Rev. Lett. **79**, 901 (1997).
[30] M. Pärnaste, M. Marcellini, and B. Hjörvarsson, J. Phys.: Condens. Matter **17**, L477 (2005).
[31] S. T. Bramwell and P. C. W. Holdsworth, J. Phys.: Condens. Matter **5**, L53 (1993).
[32] S. Hikami and T. Tsuneto, Prog. Theor. Phys. **63**, 387 (1980).
[33] R. Gupta, J. DeLapp, G. G. Batrouni, G. C. Fox, C. F. Baillie, and J. Apostolakis, Phys. Rev. Lett. **61**, 1996 (1988).
[34] J. M. Kosterlitz, J. Phys. C **7**, 1046 (1974).
[35] M. D. Stiles, Phys. Rev. B **54**, 14679 (1996).
[36] S. S. P. Parkin, N. More, and K. P. Roche, Phys. Rev. Lett. **64**, 2304 (1990).
[37] S. N. Okuno and K. Inomata, J. Phys. Soc. Jpn. **64**, 3631 (1995).
[38] S. N. Okuno and K. Inomata, Phys. Rev. Lett. **72**, 1553 (1994).
[39] G. Bayreuther, F. Bensch, and V. Kottler, J. Appl. Phys. **79**, 4509 (1996).
[40] C. Rüdt, A. Scherz, and K. Baberschke, J. Magn. Magn. Mater. **285**, 95 (2005).
[41] P. Bruno, J. Phys.: Condens. Matter **11**, 9403 (1999).
[42] H.-J. Elmers, J. Hauschild, and U. Gradmann, Phys. Rev. B **54**, 15224 (1996).
[43] L. G. Parratt, Phys. Rev. **95**, 359 (1954).
[44] V. L. Aksenov, Y. V. Nikitenko, V. V. Proglyado, M. A. Andreeva, B. Kalska, L. Häggström, and R. Wäppling, J. Magn. Magn. Mater. **258-259**, 332 (2003).
[45] A. Scherz, H. Wende, P. Poulopoulos, J. Lindner, K. Baberschke, P. Blomquist, R. Wäppling, F. Wilhelm, and N. B. Brookes, Phys. Rev. B **64**, 180407(R) (2001).
[46] C. Clavero, J. R. Skuza, Y. Choi, D. Haskel, C. Sánchez-Hanke, R. Loloee, M. Zhernenkov, M. R. Fitzsimmons, and R. A. Lukaszew, Phys. Rev. B **80**, 024418 (2009).